Parameter Boundary Characterization for DC Microgrid Islanding Detection Based on Time-Domain Voltage Oscillation Trajectory Analysis

Tianling Shi, *Student Member*, *IEEE*, Xin Xiang, *Member*, *IEEE*, Jintao Lei, Boxin Liu *Student Member*, *IEEE*, Fei Wang, *Senior Member*, *IEEE*, Li Li, Ricardo Aguilera, Wuhua Li, *Senior Member*, *IEEE*

***Abstract*- Unintentional islanding events cause potential threats to the safety of dc microgrids. Selected frequency islanding detection is considered a promising technology thanks to its good power quality and high detection accuracy. However, the conventional frequency-domain-based islanding detection parameter boundary cannot consider the impact of detection time, which causes a quite slow detection speed and thus leads to detection failure. To overcome this obstacle, a linear model of the islanding dc system is developed first to analyze the steady-state response of the voltage at the point of common coupling (PCC). On top of that, the components of the islanding system characteristic equation are analyzed based on modal analysis, which lays a good foundation for simplifying the time-domain response model of the PCC voltage. Then, the oscillation trajectory of the PCC voltage triggered by the islanding event is characterized in the time domain, which facilitates the analysis and calculation of islanding detection time. Furthermore, the boundary of the islanding detection parameters considering the detection time effect is accurately depicted to guide the resonator design. In this manner, the effect of resonant parameters on the detection time can be evaluated visually while the fast detection speed is also ensured. Finally, the proposed method is validated in simulations and hardware-in-loop experiments.**

***Index Terms*—Islanding detection, dc microgrids, oscillation trajectory, detection time, boundary characterization.**

This work was supported in part by the National Natural Science Foundation of China under Grant 52107214 and 51977126, in part by the Program of Shanghai Academic Research Leader under Grant 23XD1421100, and in part by the Zhejiang Provincial Natural Science Foundation of China under Grant LZ23E070001. (*Corresponding authors: Xin Xiang; Fei Wang.*)

Tianling Shi is with the Shanghai Key Laboratory of Power Station Automation Technology, Department of Electrical Engineering, School of Mechatronics Engineering and Automation, Shanghai University, Baoshan District, Shanghai 200444, China, and also with the School of Electrical and Data Engineering, University of Technology Sydney, Sydney, NSW 2007, Australia (e-mail: tianlingshi@shu.edu.cn).

Xin Xiang, Boxin Liu, and Wuhua Li are with the College of Electrical Engineering, Zhejiang University, Hangzhou, 310027, China (e-mail: xiangxin@zju.edu.cn; liuboxin@zju.edu.cn; woohualee@zju.edu.cn).

Fei Wang is with the Shanghai Key Laboratory of Power Station Automation Technology, Department of Electrical Engineering, School of Mechatronics Engineering and Automation, Shanghai University, Baoshan District, Shanghai 200444, China. (e-mail: f.wang@i.shu.edu.cn).

Jintao Lei is with the Corporate Research Center, Midea Group, Shanghai, China (e-mail: leijt1@midea.com).

Li Li and R. P. Aguilera are with the School of Electrical and Data Engineering, University of Technology Sydney, Sydney, NSW 2007, Australia. (e-mail: li.li@uts.edu.au; raguilera@ieee.org).

I. INTRODUCTION

The penetration of renewable energy sources, such as wind and solar, has grown rapidly in recent years to facilitate low carbon emissions and energy conservation [1]-[4]. To extensively integrate renewable distributed generators (DGs), microgrids provide an effective framework with significant autonomy [5], [6]. Since most DGs are intrinsically dc type, dc microgrids show great advantages in system controllability, conversion efficiency, and construction cost [7]-[10]. Therefore, dc microgrids have attracted much interest in future DGs-dominated power systems.

DC microgrid could experience grid-connected and islanding operation modes, where islanding is defined as a state at which the DG is disconnected from the utility grid [11]. The worst islanding condition is when the power of generation exactly neutralizes the load power, which is hard to detect due to no variation in the voltage at the point of common coupling (PCC) [12], [13]. According to IEEE standards [14], islanding events must be detected within 2 seconds, which is essential for the safety of the DG and maintenance personnel [15], [16].

In the past decades, some investigations have been conducted in dc islanding detection methods (IDMs), which are mainly classified into passive detection and active detection strategies. In the passive IDMs [17], [18], the PCC voltage is continuously monitored to allow protection devices to be triggered due to over/under voltage, but this approach is only effective under power mismatch conditions, resulting in a large non-detection zone (NDZ). To reduce the NDZ, the impedance-based IDMs [19], [20] and hybrid IDMs [3], [12] were proposed. The impedance technique detects islanding by measuring the equivalent impedance differences between grid-connected and islanding modes. However, the system equivalent impedance will vary at different operating states, which brings challenges in setting the detection threshold. The hybrid method is a two-level detection process that uses passive methods to activate active methods, but a suitable threshold is difficult to design to switch IDM. To solve this drawback, a close-loop disturbing-based IDM was first proposed in [21], where a square wave perturbation proportional to the voltage fluctuation was injected into the current signal. Once islanding occurs, the PCC voltage and current disturbance form mutual excitation, causing the voltage oscillation amplitude to reach the threshold to indicate the islanding state. Nonetheless, the disturbance model is difficult to analyze in detail due to the nonlinearity of the perturbation, making it hard to guide the islanding detection loop parameters design quantitatively.

To further address this issue, some positive feedback-based IDMs were employed to inject continuously controllable perturbation to the power or current reference command [22]-[24]. Four different schemes for implementing a positive feedback loop were evaluated in [22], where the design method of the feedback gain was analytically provided based on the Routh–Hurwitz stability criteria thanks to the linearity of the detection scheme. However, the detection mechanism of islanding events still relies on over/under voltage protection, resulting in reduced power quality and easy confusion with other faults. To improve the power quality and detection accuracy, a selected frequency islanding detection (SFID) technique was proposed [23], [24], which indicates islanding events by utilizing the frequency information perceived from the small oscillation of PCC voltage without forcing the PCC voltage beyond the normal range. With this advantage, it can make islanding events easily and readily distinguished from other grid-side events that may cause large fluctuations in PCC voltage. Moreover, the detailed oscillator parameters design is provided based on dominant eigenvalues analysis. Nonetheless, the design of islanding detection parameters in the above methods is all based on frequency-domain analysis, which cannot establish the direct relationship between islanding detection time and control parameters. As a result, the obtained parameter range can drive the PCC voltage to lose stability in islanding mode, and there are always some parameters that are invalid due to the quite slow oscillation speed. Therefore, an accurate and quantitative description is urgently required to analyze the PCC voltage dynamics in the time domain to guarantee effective and fast islanding detection.

In this paper, the SFID scheme is employed due to its good power quality and high detection accuracy. To overcome the shortcomings of the conventional parameters design method based on the frequency domain, a quantitative detection time calculation method is proposed based on the time-domain oscillation trajectory of PCC voltage to provide new constraints for accurate and fast islanding detection. The main contributions of this paper are summarized as follows:

1) The limitation of conventional islanding detection parameter boundary derived under frequency-domain constraint is revealed by developing the equivalent control model of the islanding dc system.

2) The oscillation trajectory of the PCC voltage triggered by the islanding event is characterized in the time domain to facilitate the analysis and calculation of detection time.

3) The boundary of the islanding detection parameters considering the detection time effect is accurately depicted to guide the resonator design, which guarantees effective and fast islanding detection.

The rest of this article is organized as follows. Section II first introduces a dc microgrid with SFID control and reveals the limitations of the conventional frequency domain-based design method. In Section III, the islanding detection time calculation method and the parameter boundary of SFID based on the detection time constraint are highlighted. Both simulation results and hardware-in-loop (HIL) experimental results are demonstrated in Section IV and Section V to validate the proposed method, respectively. In the end, Section VI summarizes the conclusions.

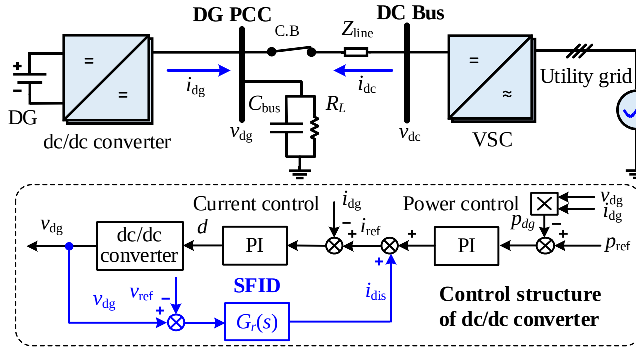

Fig. 1. Circuit of grid-connected dc microgrids and control scheme of SFID.

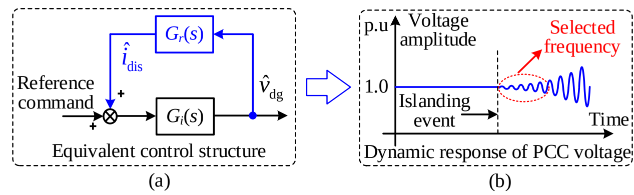

Fig. 2. Equivalent control structure and dynamic response of islanding system.

II. System Description and Modeling Analysis

This section will briefly introduce a grid-connected dc microgrid with the SFID first. Then, an equivalent circuit model is built to describe the PCC voltage dynamics. On this basis, the limitation of the conventional islanding detection parameter design method is fully illustrated.

A. System Descriptions

A typical dc microgrid with bus configuration is described in Fig. 1 [25], [26], where the DG unit is connected to a dc/dc converter to feed constant power, and the utility grid works to maintain dc bus voltage stability and system power balance through the VSC. Z_{line} represents the transmission line impedance, C_{bus} represents the equivalent bus capacitance, and the load R_L is considered as a pure resistance since it has the largest non-detection zone [27], [28].

Fig. 1 also shows the control scheme of SFID. The current disturbance is generated through a voltage positive feedback loop, where a resonant controller $G_r(s)$ given in (1) is integrated to select disturbance frequency.

$$G_r(s)=\frac{2K_r\omega_r s}{s^2+2\omega_r s+\omega_0^2} \tag{1}$$

where K_r and ω_r represent the resonant gain and bandwidth, respectively. ω_0 represents the most sensitive disturbance angular frequency.

To achieve sinusoidal oscillation at ω_0 to indicate islanding, the following amplitude and phase conditions need to be satisfied [29], [30].

$$\begin{cases} \left|A_A(\omega_0)\cdot A_F(\omega_0)\right|\ge 1 \\ \varphi_A(\omega_0)+\varphi_F(\omega_0)=2n\pi \end{cases} \tag{2}$$

where $A_A(\omega_0)$ and $\varphi_A(\omega_0)$ are the amplitude and phase of the amplification loop at ω_0, respectively; $A_F(\omega_0)$ and $\varphi_F(\omega_0)$ are the amplitude and phase of the feedback loop at ω_0, respectively.

B. Equivalent Control Structure of Islanding System

When the DG unit is disconnected from the utility grid unintentionally due to a transmission line fault, the dc system operates in the islanding mode. This condition is represented in Fig. 1 by the circuit breaker (C.B) opening. In this case, the PCC voltage dynamics is completely determined by the output voltage of the dc/dc converter and is not influenced by the ac side nonlinear load switching. Under the hardest power neutralization condition, the small signal model of DG current can be linearized as

$$\hat{i}_{\text{dg}} = sC_{\text{bus}}\hat{v}_{\text{dg}} + \hat{v}_{\text{dg}}/R_{\text{L}} \tag{3}$$

where i_{dg} is the DG output current, and v_{dg} is the PCC voltage.

According to Fig. 1, under continuous current disturbances, the dynamics of the reference current is expressed as

$$\hat{i}_{\text{ref}} = \left(K_{pp} + K_{pi}/s\right)(\hat{p}_{\text{ref}} - \hat{p}_{\text{dg}}) + \hat{i}_{\text{dis}} \tag{4}$$

where K_{pp} and K_{pi} are the proportion and integral coefficients of the power PI controller, respectively, p_{ref} is the DG power reference, and the DG output power p_{dg} can be linearized as

$$\hat{p}_{\text{dg}} = I_0\hat{v}_{\text{dg}} + V_0\hat{i}_{\text{dg}} \tag{5}$$

where V_0 and I_0 are the steady-state voltage and current of the PCC, respectively.

According to TABLE I, the bandwidth of the current loop is 1.2kHz, and the bandwidth of the outer power loop is 70Hz. Since the PCC voltage in the islanding mode is most sensitive to low-frequency current disturbance [24], [25], the inner current loop could be simplified as (6), which would not have much effect on the oscillation characterization of PCC voltage.

$$\hat{i}_{\text{dg}} = \hat{i}_{\text{ref}} \tag{6}$$

Then, in the power neutralization islanded scenario where $V_0 = R_{\text{L}}I_0$, by solving (3)-(6), the amplification loop can be modeled as

$$G_i(s) = \frac{\hat{v}_{\text{dg}}}{\hat{i}_{\text{dis}}} = \frac{a_1 s}{b_2 s^2 + b_1 s + b_0} \tag{7}$$

where

$$\begin{cases} a_1 = R_{\text{L}} \\ b_2 = C_{\text{bus}}R_{\text{L}} + C_{\text{bus}}R_{\text{L}}V_0K_{pp} \\ b_1 = 1 + 2V_0K_{pp} + C_{\text{bus}}R_{\text{L}}V_0K_{pi} \\ b_0 = 2V_0K_{pi} \end{cases} \tag{8}$$

According to the SFID scheme presented in Fig. 1, the current disturbance can be derived as

$$\hat{i}_{\text{dis}} = G_r(s)\hat{v}_{\text{dg}} \tag{9}$$

Thus, the control structure of the islanding system under continuous current disturbances can be equivalent to Fig. 2(a), and the PCC voltage dynamics can be described as (10). With the SFID, the PCC voltage aims to show a sinusoidal oscillatory response in islanding modes, as shown in Fig. 2(b).

$$\Phi(s) = \frac{G_i(s)}{1 - G_i(s)G_r(s)} \tag{10}$$

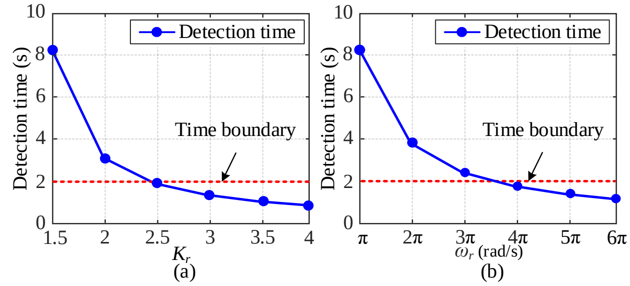

Fig. 3. Detection time variation with K_r and ω_r changing.

C. Limitations of Conventional Boundary

The conventional design method of islanding detection parameters usually takes the islanding system stability boundary as the criterion [22]-[25]. To analyze the marginal stability of the islanding dc microgrid, inserting (1) and (7) into (10), the characteristic equation can be obtained as

$$\begin{aligned} & b_2 s^4 + (2b_2\omega_r + b_1)s^3 + \left(b_2\omega_0^2 + 2b_1\omega_r + b_0 - 2a_1K_r\omega_r\right)s^2 \\ & + \left(b_1\omega_0^2 + 2b_0\omega_r\right)s + b_0\omega_0^2 = 0 \end{aligned} \tag{11}$$

where ω_0 is expressed as follows [30].

$$\omega_0 = \sqrt{\frac{2i_{\text{dg}}K_{pi}}{C_{\text{bus}}\left(1 + V_0K_{pp}\right)}} \tag{12}$$

Then, according to the Routh–Hurwitz stability criteria, the boundary of K_r and ω_r for marginal stability of the islanding system is derived as

$$\begin{cases} K_r \geq \left(1 + 2V_0K_{pp} + CR_LV_0K_{pi}\right)/R_L \\ \omega_r > 0 \end{cases} \tag{13}$$

However, this frequency-domain-based boundary is not a sufficient condition for successful islanding detection due to the detection time is not taken into consideration. To further demonstrate this issue, the variation trends of islanding detection time with K_r and ω_r changing are described in Fig. 3 based on the time-domain simulation parameters given in TABLE I. As shown in Fig. 3(a), ω_r is set to be π rad/s, and the detection time decreases as K_r increases. When K_r is smaller than 2.5, the detection time is larger than 2 seconds. Similarly, when K_r is 1.5, ω_r is set to at least 4π rad/s to ensure successful detection within 2 seconds, as presented in Fig. 3(b). This means that when using conventional design methods, there is always a potential combination of K_r and ω_r that makes the DG unit unable to provide accurate detection information for islanding protection within the required 2 seconds. Thus, detection time will be further analyzed and calculated in the following section to guide the SFID design.

III. Oscillating Trajectory Characterization and Detection Time Calculation

In this section, the islanding system characteristic equation are analyzed first to simplify the time-domain model of PCC voltage. Then, the time-domain oscillation trajectory of the PCC voltage is characterized to facilitate the calculation of detection time. Furthermore, the boundary of islanding detection parameters considering the detection time effect is depicted to guide the SFID design. In this manner, the impact mechanism of detection time can be revealed while the fast detection speed is also ensured.

A. Analysis of Characteristic Equation

According to (1), (7) and (10), the PCC voltage dynamics $\Phi(s)$ can be expanded as

$$\Phi(s)=\frac{A_3s^3+A_2s^2+A_1s}{s^4+B_3s^3+B_2s^2+B_1s+B_0} \tag{14}$$

where

$$\begin{cases}A_3=a_1/b_2\\A_2=2a_1\omega_r/b_2\\A_1=a_1\omega_0^2/b_2\\B_3=(2b_2\omega_r+b_1)/b_2\\B_2=\left(b_2\omega_0^2+2b_1\omega_r+b_0-2a_1K_r\omega_r\right)/b_2\\B_1=\left(b_1\omega_0^2+2b_0\omega_r\right)/b_2\\B_0=b_0\omega_0^2/b_2\end{cases} \tag{15}$$

The high-order characteristics of (14) bring great challenges to the time-domain analysis. To simplify further, the high-order characteristic equation is written as a combination of standard second-order equations in the following.

$$\left(s^2+\alpha s+\beta\right)\left(s^2+\gamma s+\delta\right)=0 \tag{16}$$

As for a standard second-order system, β and δ are positive; thus, α and γ determine the damping ratio of the system. Then (16) can be expanded as

$$s^4+(\alpha+\gamma)s^3+(\beta+\alpha\gamma+\delta)s^2+(\alpha\delta+\beta\gamma)s+\beta\delta=0 \tag{17}$$

where

$$\begin{cases}\alpha+\gamma=B_3\\\beta+\alpha\gamma+\delta=B_2\\\alpha\delta+\beta\gamma=B_1\\\beta\delta=B_0\end{cases} \tag{18}$$

Solving the four equations in (17), we can obtain six roots of coefficient α. Ignore the imaginary roots and retain the two real roots as

$$\begin{cases}\alpha_1=\frac{1}{2}B_3-\frac{1}{2}\sqrt{B_3^2-4\left(\frac{2B_2}{3}-\frac{2^{1/3}G_2}{3G_1}-\frac{G_1}{3\times2^{1/3}}\right)}\\\alpha_2=\frac{1}{2}B_3+\frac{1}{2}\sqrt{B_3^2-4\left(\frac{2B_2}{3}-\frac{2^{1/3}G_2}{3G_1}-\frac{G_1}{3\times2^{1/3}}\right)}\end{cases} \tag{19}$$

where G_1 is defined as follows

$$G_1=\left(G_3+\sqrt{G_3^2-4G_2^3}\right)^{1/3} \tag{20}$$

In addition, G_2 and G_3 in (19) and (20) are expressed as

$$G_2=B_2^2-3B_3B_1+12B_0 \tag{21}$$

$$G_3=2B_2^3+27B_3^2B_0+27B_1^2-9B_3B_2B_1-72B_2B_0 \tag{22}$$

Similarly, the solution of coefficient γ has the same form as α. It can be clearly seen from (19) that $\alpha_2>0$, but the characteristic of α_1 requires further analysis. According to the mechanism of SFID, PCC voltage dynamics is a divergent oscillation process with a particular frequency. This means that the islanding system poses negative damping. That is to say, α_1 must be negative, otherwise the system is stable.

Assuming that $\alpha<0$, $\gamma>0$, and thus $\alpha=\alpha_1$, $\gamma=\alpha_2$. In this case, β and δ are derived as

$$\beta=\beta_1=\frac{\alpha_2\alpha_1^2-B_2\alpha_1+B_1}{\alpha_2-\alpha_1} \tag{23}$$

$$\delta=\beta_2=\frac{B_0(\alpha_2-\alpha_1)}{\alpha_2\alpha_1^2-B_2\alpha_1+B_1} \tag{24}$$

B. Oscillation Trajectory-Based Detection Time Calculation

In the dc microgrid model, the occurrence of islanding is emulated by manually disconnecting the C.B. To characterize the oscillating trajectory of PCC voltage triggered by an islanding event, a step-perturbation is used to simulate islanding events and describe the system dynamic response. Thus, the PCC voltage $\Phi'(s)$ triggered by the islanding event can be calculated by multiplying $\Phi(s)$ with the Laplace function of the unit step as follows.

$$\Phi'(s)=\frac{1}{s}\Phi(s)=\frac{A_3s^2+A_2s+A_1}{\left(s^2+\alpha_1s+\beta_1\right)\left(s^2+\alpha_2s+\beta_2\right)} \tag{25}$$

To facilitate time-domain analysis, (25) can be factored as

$$\Phi'(s)=\frac{\lambda_1s+\eta_1}{s^2+\alpha_1s+\beta_1}+\frac{\lambda_2s+\eta_2}{s^2+\alpha_2s+\beta_2} \tag{26}$$

where

$$\begin{cases}\lambda_1=\frac{A_3(\alpha_2\beta_1-\alpha_1\beta_2)+A_2(\beta_2-\beta_1)+A_1(\alpha_1-\alpha_2)}{\beta_1^2+\beta_1\alpha_2^2+\beta_2\alpha_1^2+\beta_2^2-\alpha_1\alpha_2\beta_1-\alpha_1\alpha_2\beta_2-2\beta_1\beta_2}\\\lambda_2=-\frac{A_3(\alpha_2\beta_1-\alpha_1\beta_2)+A_2(\beta_2-\beta_1)+A_1(\alpha_1-\alpha_2)}{\beta_1^2+\beta_1\alpha_2^2+\beta_2\alpha_1^2+\beta_2^2-\alpha_1\alpha_2\beta_1-\alpha_1\alpha_2\beta_2-2\beta_1\beta_2}\\\eta_1=\\\quad\frac{A_3\left(\beta_1^2-\beta_1\beta_2\right)+A_2(\alpha_2\beta_1-\alpha_1\beta_1)+A_1\left(\alpha_1^2+\beta_2-\alpha_1\alpha_2-\beta_1\right)}{\beta_1^2+\beta_1\alpha_2^2+\beta_2\alpha_1^2+\beta_2^2-\alpha_1\alpha_2\beta_1-\alpha_1\alpha_2\beta_2-2\beta_1\beta_2}\\\eta_2=\\\quad\frac{A_3\left(\beta_2^2-\beta_1\beta_2\right)+A_2(\alpha_1\beta_2-\alpha_2\beta_2)+A_1\left(\alpha_2^2+\beta_1-\alpha_1\alpha_2-\beta_2\right)}{\beta_1^2+\beta_1\alpha_2^2+\beta_2\alpha_1^2+\beta_2^2-\alpha_1\alpha_2\beta_1-\alpha_1\alpha_2\beta_2-2\beta_1\beta_2}\end{cases} \tag{27}$$

Take the inverse Laplace transform of (26) and further discuss two cases. If each characteristic equation has two real roots, the PCC voltage amplitude in the time domain will rise exponentially without oscillation, which is a simple and fast special detection case that is not discussed in detail in this article. In another general case, each characteristic equation has a pair of conjugate roots, and the PCC voltage in the time-domain model can be described as

$$\begin{aligned}\Phi'(t)=&\lambda_1e^{-\alpha_1t/2}\cos\left(\omega_{p1}t\right)+\frac{\eta_1}{\omega_{p1}}e^{-\alpha_1t/2}\sin\left(\omega_{p1}t\right)\\&+\lambda_2e^{-\alpha_2t/2}\cos\left(\omega_{p2}t\right)+\frac{\eta_2}{\omega_{p2}}e^{-\alpha_2t/2}\sin\left(\omega_{p2}t\right)\end{aligned} \tag{28}$$

where ω_{p1} and ω_{p2} are the oscillation angular frequency.

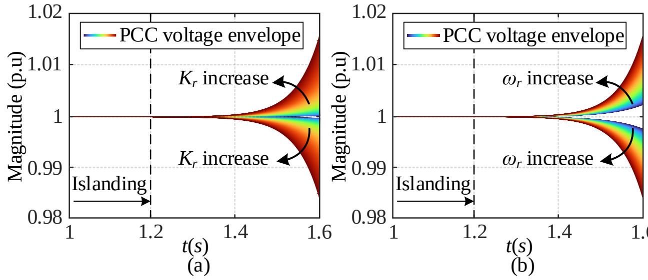

Fig. 4. Impact of K_r and ω_r variation on the PCC voltage envelope.

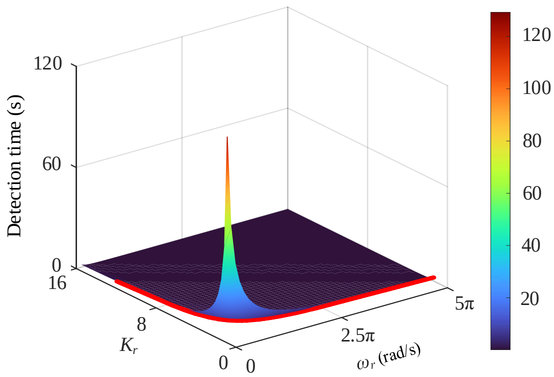

Fig. 5. Detection time variation with resonant parameters changing.

According to the previous analysis, α_1 is negative and α_2 is positive, which means that the amplitude of $e^{-\alpha_2 t/2}$ decreases with time increasing, and the maximum amplitude appears close to the beginning. Since the standard for SFID to indicate an islanding condition is to detect three consecutive oscillation cycles whose frequency agrees with the disturbance frequency, the amplitude of $e^{-\alpha_2 t/2}$ at that moment has attenuated close to zero. Thus, the last two terms can be ignored in (28), and ω_{p1} is called the practical oscillation angular frequency as defined in (29). It is also worth noting that $(4\beta_1-\alpha_1^2)>0$ when the system has a pair of conjugate roots.

$$\omega_{p1}=\frac{1}{2}\sqrt{4\beta_1-\alpha_1^2} \tag{29}$$

Hence, the oscillating trajectory of PCC voltage in time domain can be rewritten as

$$\Phi'(t)=\lambda_1 e^{-\alpha_1 t/2}\cos(\omega_{p1}t)+\frac{\eta_1}{\omega_{p1}}e^{-\alpha_1 t/2}\sin(\omega_{p1}t) \tag{30}$$

It can be seen from (30) that gaining the exact solution of time t is quite difficult since it involves both amplitude and frequency parts. According to the detection principle of SFID, the detection time is determined by the oscillation start time, which is indicated by the amplitude threshold. Thus, the detection time problem can be transformed into calculating the time for the PCC voltage amplitude envelope to reach the target threshold. The envelope equation of $\Phi'(t)$ is given by

$$\Psi(t)=\pm\sqrt{\lambda_1^2+(\eta_1/\omega_{p1})^2}\,e^{-\alpha_1 t/2} \tag{31}$$

Assume that the voltage fluctuation threshold is set to n V to indicate the occurrence of oscillation. It is worth noting that the oscillation threshold should be larger than the voltage ripple to avoid power quality problems caused by the ripple [31], [32] that affect islanding detection and detection time

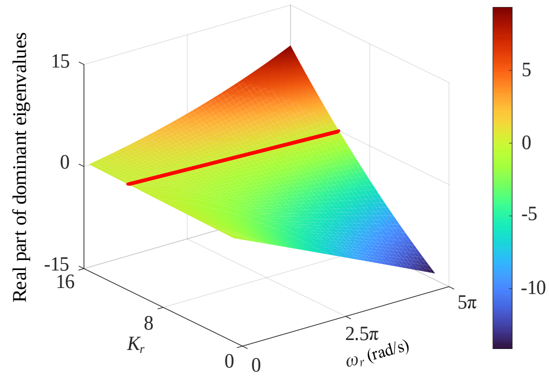

Fig. 6. Dominant eigenvalues variation with resonant parameters changing.

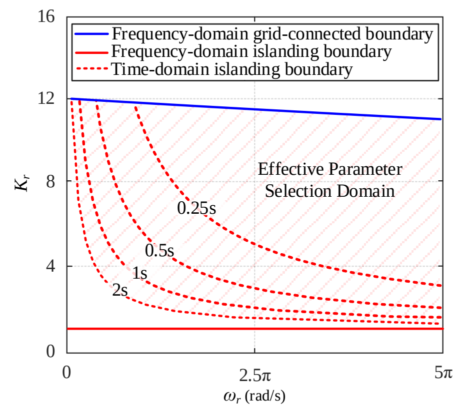

Fig. 7. Effective parameters selection-domain.

calculation. Thus, when the amplitude of PCC voltage rises to n V and experiences three consecutive oscillation cycles, the detection time can be calculated as

$$\Delta t=-\frac{2}{\alpha_1}\ln\left(n\omega_{p1}\Big/\sqrt{\omega_{p1}^2\lambda_1^2+\eta_1^2}\right)+\frac{6\pi}{\omega_{p1}} \tag{32}$$

It can be obtained from (32) that the detection time is determined by the α_1. According to (15) and (19), for a known system, α_1 a is a function composed of K_r, ω_r and ω_0. The design method of ω_0 has been given in (12), and thus the value of α_1 is determined by K_r and ω_r. To make the PCC voltage oscillate in the islanding mode and reach the set amplitude threshold within 2 seconds, the detection time analysis and islanding detection parameters design considering the impact of detection time will be given in the following.

C. Parameter Boundary Characterization

The envelope curves of PCC voltage with different K_r and ω_r are presented in Fig. 4. It can be seen from Fig. 4(a) that the growth rate of the envelope becomes faster with K_r rising due to the increase of the exponent $-\alpha_1$. This means that with a large K_r, the PCC voltage reaches the amplitude threshold quickly, and thus the required detection time is less. Similarly, with K_r set as a constant, Fig. 4(b) shows that increasing ω_r can also improve the rise rate of PCC voltage envelope, which contributes to improving the detection speed.

According to (32), the relationship among detection time, K_r, and ω_r is further demonstrated in Fig. 5. It can be seen from this figure that the detection time decreases as K_r increases from 0 to 16 and ω_r rises from 0 to 5π rad/s, which thanks to the increasing growth rate of the PCC voltage amplitude shown in Fig. 4. The effective detection time boundary is indicated by the red line in Fig. 5, and the case above this line means that the islanding event can be detected within 2 seconds.

It is worth noting that the design principle of the islanding detection loop is to make the PCC voltage oscillate during islanding events but maintain stable operation at grid-connected states. Thus, the dominant eigenvalue analysis is employed to describe the stability boundary of the grid-connected system in the following.

When the DG operates in grid-connected modes, according to Fig. 1, the dynamics of i_{dc} is described as

$$\hat{i}_{\mathrm{dc}} = -\hat{v}_{\mathrm{dg}} / \left(R_{\mathrm{line}} + sL_{\mathrm{line}}\right) \tag{33}$$

where R_{line} and L_{line} represent the resistance and inductance of dc grid transmission line, respectively.

Then, the current balance equation is rewritten as

$$\hat{i}_{\mathrm{dg}} + \hat{i}_{\mathrm{dc}} = sC_{\mathrm{bus}}\hat{v}_{\mathrm{dg}} + \hat{v}_{\mathrm{dg}} / R_{\mathrm{L}} \tag{34}$$

Solving (4)-(6), (33) and (34), the disturbance model in grid-connected modes will be

$$G_c\left(s\right) = \frac{\hat{v}_{\mathrm{dc}}}{\hat{i}_{\mathrm{dis}}} = \frac{a_2 s^2 + a_1 s}{b_3 s^3 + b_2 s^2 + b_1 s + b_0} \tag{35}$$

where

$$\begin{cases} a_2 = R_{\mathrm{L}} L_{\mathrm{line}} \\ a_1 = R_{\mathrm{L}} R_{\mathrm{line}} \\ b_3 = C_{\mathrm{bus}} L_{\mathrm{line}} R_{\mathrm{L}} + C_{\mathrm{bus}} K_{pp} L_{\mathrm{line}} R_{\mathrm{L}} V_0 \\ b_2 = L_{\mathrm{line}} + C_{\mathrm{bus}} R_{\mathrm{line}} R_{\mathrm{L}} + C_{\mathrm{bus}} K_{pp} R_{\mathrm{line}} R_{\mathrm{L}} V_0 \\ \quad + C_{\mathrm{bus}} K_{pi} L_{\mathrm{line}} R_{\mathrm{L}} V_0 + 2K_{pp} L_{\mathrm{line}} V_0 \\ b_1 = R_{\mathrm{line}} + R_{\mathrm{L}} + K_{pp} R_{\mathrm{L}} V_0 + C_{\mathrm{bus}} K_{pi} R_{\mathrm{line}} R_{\mathrm{L}} V_0 \\ \quad + 2K_{pp} R_{\mathrm{line}} V_0 + 2K_{pi} L_{\mathrm{line}} V_0 \\ b_0 = K_{pi} V_0 R_{\mathrm{L}} + 2K_{pi} V_0 R_{\mathrm{line}} \end{cases} \tag{36}$$

Thus, the dynamics of PCC voltage in grid-connected modes can be described as

$$T\left(s\right) = \frac{G_c\left(s\right)}{1 - G_r\left(s\right) \cdot G_c\left(s\right)} \tag{37}$$

For different combinations of K_r and ω_r, the dominant eigenvalues of (37) are calculated in Fig. 6. The stability boundary of the grid-connected system is indicated by a red line, and the conditions corresponding to the area below this line represent that the PCC voltage can preserve stability in the grid-connected mode.

Based on Fig. 5 and Fig. 6, the effective parameters selection domain of K_r and ω_r are described between the blue grid-connected boundary line and red dashed islanding boundary line, as shown in the shadow area of Fig. 7. It also can be seen that as the target detecting time reduces, the effective parameter selection domain will narrow. Then, the conventional frequency-domain-based islanding boundary derived according to (13) is shown by the red solid line in Fig. 7. Compared with the conventional method, time-domain-based islanding boundary can provide a more accurate and effective parameters selection domain. This is reflected more clearly when pursuing faster detection speed, because the invalid parameter selection range based on the frequency domain expands as the detection time decreases. Therefore, the quantitative relationships between the detection time and resonant parameters obtained from the voltage oscillation trajectory can effectively guide the detection loop design and detection speed regulation.

IV. Simulation Verification

To verify the accuracy and effectiveness of the proposed islanding detection calculation method, an 80kW, 400V time-domain model of grid-connected dc microgrid is built. The detailed parameters of the dc system are given in TABLE I. Firstly, the proposed analytical calculation method is validated during islanding events. Also, the stability boundaries of the islanding system and grid-connected system are verified. Then, the effect of changes in system power and resonant parameters is evaluated. Moreover, the advantages of the proposed time-domain-based design method are proved by comparative study. Finally, the described parameter domain is validated in a two-DG system.

TABLE I
Parameters of Grid-connected DC Microgrid

Category	Parameters	Value
DC grid	Rated bus voltage V_{dc}	400V
	Impedance of transmission line Z_{line}	0.2Ω/0.3mH
Load	Rated resistance R_{L}	2Ω
DG	Rated output power P_{dg}	80kW
	Equivalent bus capacitance C_{bus}	2000μF
	Switching frequency	10kHz
	Proportion item of power controller K_{pp}	2×10^{-5}
	Integral item of power controller K_{pi}	0.84
	Proportion item of current controller K_{ip}	0.0125
	Integral item of current controller K_{ii}	18.6
VSC	DC-link smoothing capacitor C_{dc}	1880μF
	Proportion item of voltage controller K_{vp}	0.1
	Integral item of voltage controller K_{vi}	25
	Proportion item of current controller K_{cp}	25
	Integral item of current controller K_{ci}	3

A. Validation of Calculation Methods

To validate the proposed oscillation trajectory-based islanding detection time calculation methods, the simulated and calculated dynamic responses are shown in Fig. 8 where both the DG unit and load operate at the rated power neutralization condition. K_r is selected as 5, ω_r is set as 3π rad/s, and f_0 ($f_0=\omega_0/2\pi$) is set as 65Hz according to (12). As shown in Fig. 8(a), when islanding happens at t=1.2s, the PCC voltage presents a divergent oscillatory response due to the absence of voltage support. The time-domain simulation waveform and the analytical calculation results of PCC voltage are presented in a blue solid line and red dashed line in Fig. 8(a), respectively. It clearly shows that calculation waveforms match exactly with simulation results, which indicates the correctness of the oscillating trajectory function (30). Meanwhile, Fig. 8(b) shows the oscillation frequency is 65Hz, which matches extremely well with the theoretical

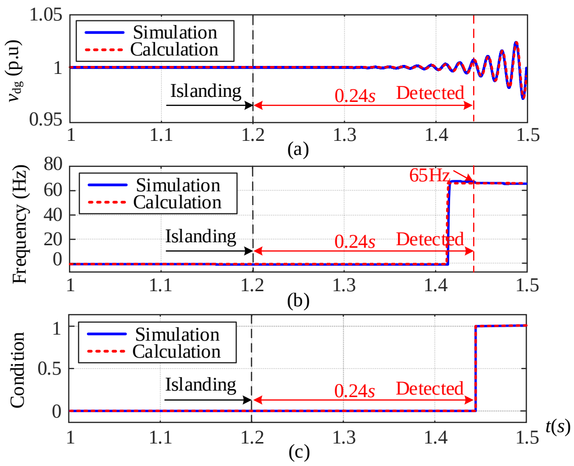

Fig. 8. Simulated and calculated dynamic responses of the islanding system.

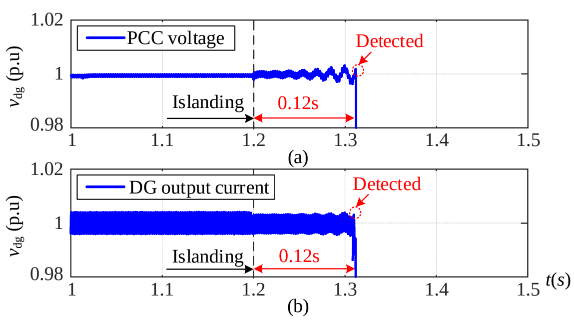

Fig. 9. Islanding detection performance under large voltage ripple conditions

resonant frequency. This is the most significant advantage of the SFID because accurate frequency information allows the dc microgrid to detect islanding events rapidly and avoid severe voltage fluctuations. When the system detects three consecutive oscillation cycles and the oscillation frequency is consistent with the selected resonant frequency, it indicates the occurrence of islanding. As presented in Fig. 8(c), the dc system costs 0.24s to successfully detect islanding event, and the detection time calculated by the envelope solution is also 0.24s. Moreover, This case validates the accuracy of the proposed detection time calculation method.

Then, with the same K_r and ω_r, a case in which the voltage ripple is three times larger than that in Fig. 8(a) is tested to demonstrate the impact of power quality on the proposed method. As shown in Fig. 9, the PCC voltage and DG output current present significant fluctuations in the grid-connected mode. When islanding occurs, the voltage oscillation is more severe than in Fig. 8(a). When the islanding is detected, the DG stops supplying power to the dc system. It is obvious that the detection time is much shorter than that in Fig. 8 because the large voltage ripple increases the disturbance sensitivity. Thus, the power quality would not affect the effectiveness of the described parameter range.

B. *Validation of Stability Boundary*

In this test, ω_r is set to 4π rad/s, and K_r is set to the critical stable value of the islanding system and grid-connected system according to Fig. 7 to assess the described stability boundaries. As displayed in Fig. 10(a), when K_r is set to 1.4,

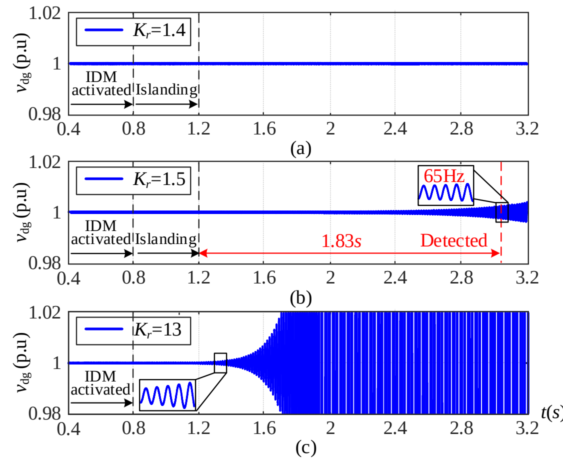

Fig. 10. Stability boundaries validation.

the PCC voltage is stable at both grid-connected states and islanding states. Then, when K_r is increased to 1.5, Fig. 10(b) shows that v_{dg} also preserves stability at the initial grid-connected state. However, once the islanding happens, the PCC voltage presents a divergent oscillation response, and the islanding condition is detected within 2 seconds. Furthermore, when K_r is increased to 13, the disturbance component is significantly strengthened, which causes the system to lose stability in the grid-connected mode, as shown in Fig. 10(c). The abovementioned cases prove that the practical stability boundaries are consistent with the analytical results.

C. *Impact of DG and Load Power*

Since the output power of DG is random, this case will test the impact of system power on detection time. In the rated power case, K_r is selected as 3 and ω_r is set as 4π rad/s, the successful islanding detection costs 0.27s and the practical oscillation agrees with the disturbance frequency 65Hz, as presented in Fig. 11(a) and Fig. 12(a). Then, when both the power of DG and load decreases to 0.75 p.u, the DG output current i_{dg} is sampled and substituted into (12) to update the ω_0, and thus the resonant frequency is adaptively adjusted to 56Hz. As can be seen from Fig. 11(b) and Fig. 12(b), the analytical dynamics of PCC voltage could remain in line with the simulation waveforms in the face of different operation states, and the detection time only takes 0.25s. When the system power continues to decrease to 50% of the rated power, the increase in voltage oscillation amplitude causes the detection time to be further reduced, as shown in Fig. 11(c). Meanwhile, as the resonant frequency is updated to 46Hz, the actual oscillation frequency also tends to 46Hz, as presented in Fig. 12(c). Finally, when the DG operates under the rated condition and load power is 1.25 p.u, the PCC voltage drops rapidly to the undervoltage threshold of 0.88 p.u to indicate an islanding event, as shown in Fig. 11(d). Thus, the islanding detection parameter boundary obtained in this paper can effectively ensure accurate and fast islanding detection under different DG power conditions.

D. *Impact of Resonant Gain and Resonant Bandwidth*

In addition to the system power, both resonant gain K_r and resonant bandwidth ω_r also have a great impact on the

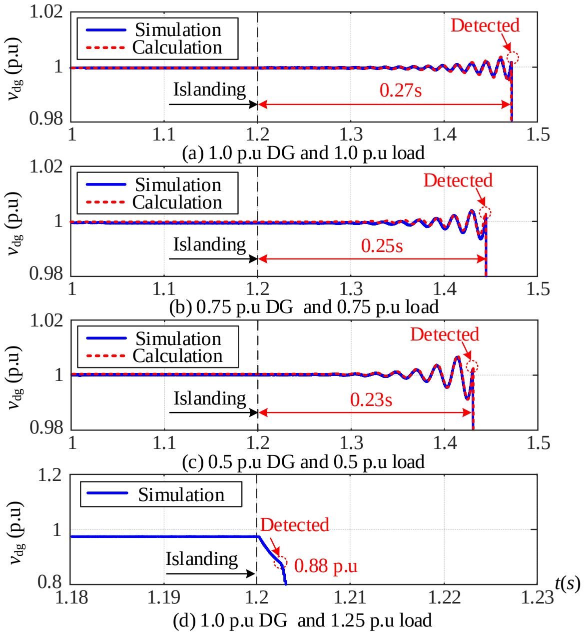

Fig. 11. Simulated and calculated dynamic responses of PCC voltage with different system power.

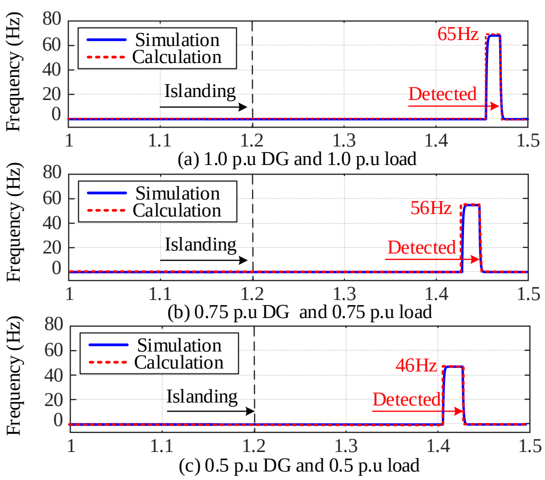

Fig. 12. Simulated and calculated oscillation frequency information with different system power.

islanding time. Fig. 13 displays the dynamic response of PCC voltage with different K_r during islanding events. In this case, ω_r is 5π rad/s, and K_r increases from 3 to 5. As shown in Fig. 13(a) to (c), the calculated dynamic responses of the three cases fit extremely well with the simulation results, indicating the accuracy of detection dime calculation. Moreover, the oscillation amplitude of v_{dg} turns to be larger as K_r rises, which also agrees with the envelop-based oscillation amplitude analysis in Fig. 4(a) and means a faster detection speed. Then, K_r is selected as 6, and ω_r is set to rise from 3π rad/s to 5π rad/s to explore the effect of ω_r on the dynamic response of PCC voltage. As shown in Fig. 14(a) to (c), the oscillation amplitude keeps increasing significantly, and the detection time is decreased. In consequence, the detection speed can be greatly enhanced by increasing resonant gain and resonant bandwidth as long as ensuring their values are in the effective parameter selection domain in Fig. 7.

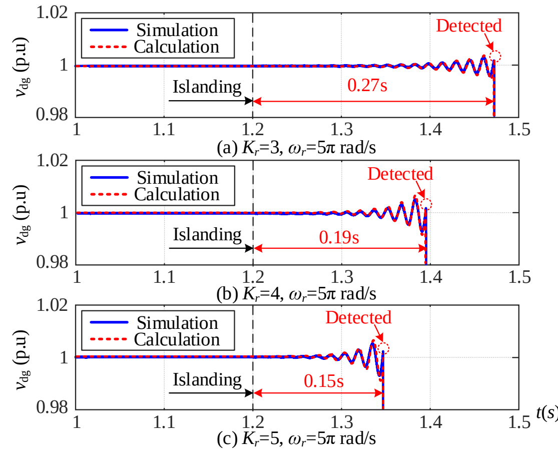

Fig. 13. Simulated and calculated dynamic responses of PCC voltage with different K_r during islanding events.

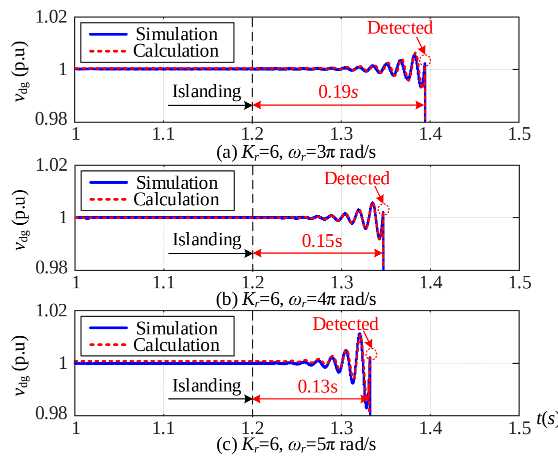

Fig. 14. Simulated and calculated dynamic responses of PCC voltage with different ω_r during islanding events.

E. Comparative Study

To further verify the advantages of the proposed time-domain-based design method in accuracy and detection time for the SFID, a comparative study is carried out in Fig. 15. Firstly, K_r is selected as 2, and ω_r is selected as π rad/s, which satisfies the conventional parameters selection domain obtained form (13) based on frequency-domain. As shown in Fig. 15(a), the PCC voltage loses stability during islanding events, but the DG cannot detect the islanding event within the maximum 2 seconds required by the IEEE standards. Thus, conventional frequency-domain-based design techniques make the detection time could not be designed accurately and even still cause failure in islanding detection, resulting in damage to equipment and injuries to maintenance personnel. According to the proposed time-domain method, when ω_r is π rad/s, the marginal value of K_r that guarantees a detection time of 2 seconds is 2.4, which effectively avoids invalid parameter ranges. Then, K_r is increased to 2.5, and it can be seen from Fig. 15(b) that the successful islanding detection costs only 1.91 seconds. The comparison results show that the proposed time-domain method provides higher detection accuracy and faster detection speed than conventional techniques.

It is also worth noting that the islanding detection parameter domain is described under resistive load conditions, which is

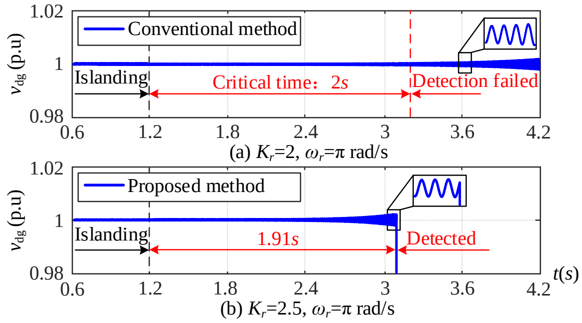

Fig. 15. Comparative simulation results of accuracy and detection time.

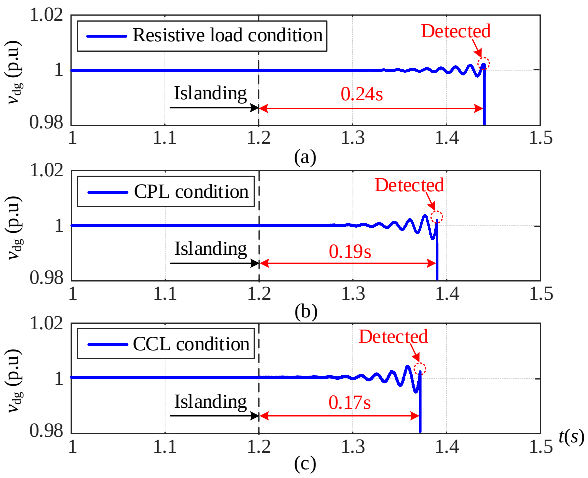

Fig. 16. Comparison of detection time under different load conditions.

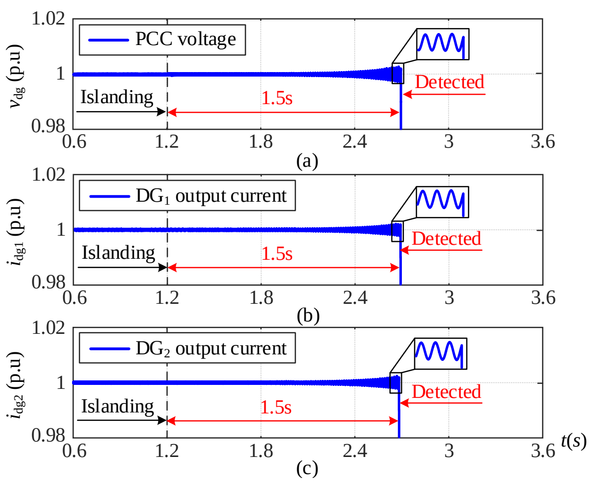

Fig. 17 Detection time of a two-DG system when K_r is 2.4 and ω_r is π rad/s

the most difficult case for islanding detection in dc microgrids. To demonstrate the effectiveness of the described parameter selection domain, constant power load (CPL) and constant current load (CCL) conditions are considered for testing the islanding detection performance. Setting K_r to be 5 and ω_r to be 3π rad/s, it can be seen from Fig. 16(a) that the detection time is 0.24s. However, with the same K_r and ω_r, the detection time under CPL and CCL conditions only needs 0.19s and 0.17s, respectively, as shown in Fig. 16(b) and Fig. 16(c). This means that the islanding detection parameter boundary characterized under pure resistive load conditions is the most conservative and is also effective for other load types.

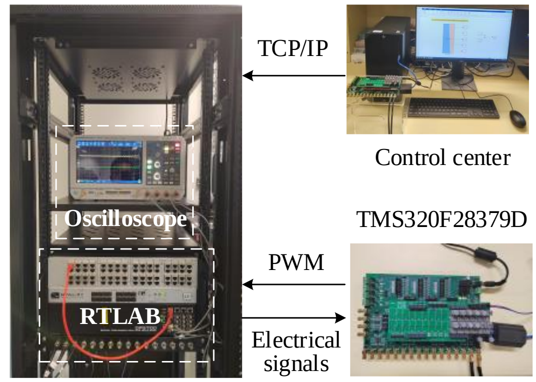

Fig. 18. HIL experimental setup.

F. *Multiple Sources Test*

Finally, the effectiveness of the described islanding detection parameters domain is also tested in a two-DG system with bus configuration [30]. According to Fig. 7, when ω_r is π rad/s, K_r corresponding to the critical detection time 2s is 2.4 for a single DG system. However, Fig. 17 shows that in the two-DG system, islanding detection only needs 1.5s with the same K_r and ω_r. The detection speed of the multi-DG system is much faster than that of the single DG system because multiple DGs participate in perturbing the PCC voltage at the same time. Thus, the parameter boundary for dc microgrid islanding detection described under a single DG system can provide conservative constraints to ensure that the system with multiple sources can also effectively and readily detect islanding events.

V. Experimental Validation

To further verify the correctness of the theoretical analysis and simulation results, a HIL experimental platform with the same parameters as time-domain simulations is built in the laboratory, as shown in Fig. 18. The power components including dc/dc converter and VSC are emulated by the RTLAB 5700. The SFID algorithm is downloaded to a TI TMS320F28379D digital signal processor (DSP) to test its performance. The designed DSP controller features a 32-bit C28x CPU core, which offers high computational performance and efficiency for real-time control. Moreover, the TMS320F28379D can operate within a wide voltage range of 1.71V to 3.6V, allowing it to generate the required gate-switching pulses to control the dc/dc converter in RTLAB.

A. *Validation of Calculation Methods*

The accuracy of the proposed analytical calculation method is first evaluated in Fig. 19, where the analytical results of oscillation trajectory are also depicted in the same figure with a red dashed line for comparison. It can be seen that when an islanding event happens, the PCC voltage presents a divergent oscillation at 65 Hz, and the analytical results agree with the experimental waveform exactly. It is noted that after successful detection, the DG stops supplying power to the local load. As shown in Fig. 19, it takes 0.24 seconds to detect islanding in this case, which is consistent with the theoretical calculation results. Moreover, Fig. 19 shows that the voltage

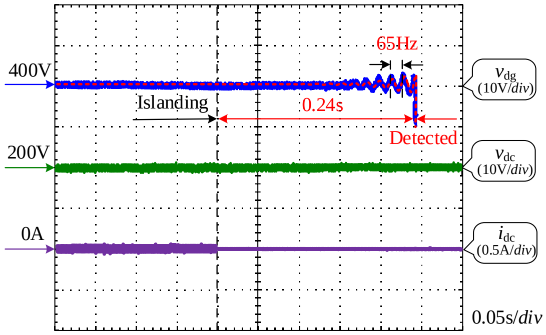

Fig. 19. Experimental and calculated dynamic response results during islanding events.

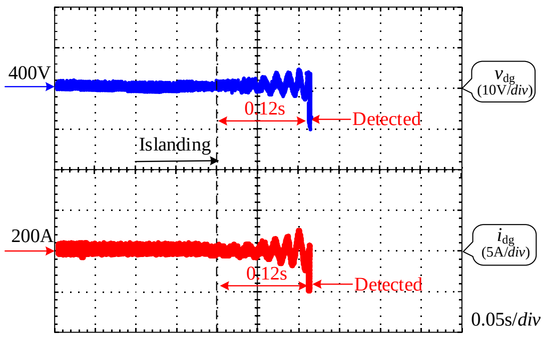

Fig. 20. Experimental results under large voltage ripple conditions.

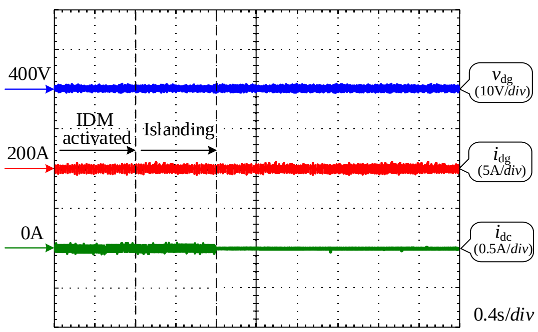

Fig. 21. Experimental and calculated dynamic responses in the islanding mode when ω_r is 4π rad/s and K_r is 1.4.

fluctuation when the detection is successful is only 0.01 p.u, indicating the advantage of the SFID method in power quality. Thus, the correctness of the oscillation trajectory characterizing and detection time calculation for the SFID has been verified again.

Then, the voltage ripple is increased to test the effectiveness of the proposed method. It can be seen from Fig. 20 that the PCC voltage and DG output current show significant fluctuations in the grid-connected mode, which means that the voltage difference sent to the resonant controller will be larger and the disturbance will be enhanced. As a result, the detection speed is much faster than that in Fig. 19. Thus, the proposed parameter design method would not limited by the power quality.

B. Validation of Stability Boundary

Then, three different cases are tested to evaluate the correctness of the stability boundaries. In the first case, K_r and ω_r are set to 1.4 and 4π rad/s, respectively, as this parameter combination is below the stability boundary of the islanding

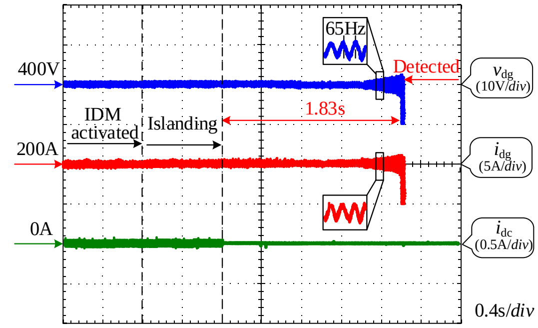

Fig. 22. Experimental and calculated dynamic responses in the islanding mode when ω_r is 4π rad/s and K_r is 1.5.

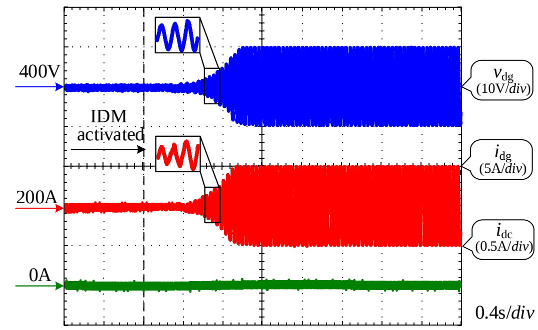

Fig. 23. Experimental and calculated dynamic responses in the grid-connected mode when ω_r is 4π rad/s and K_r is 13.

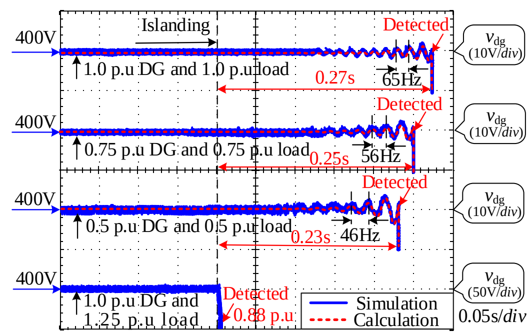

Fig. 24. Experimental and calculated dynamic responses of PCC voltage with different system power.

system, as described in Fig. 7. When islanding occurs, Fig. 21 shows that the PCC voltage v_{dg} does not have any fluctuation due to the neutralization between DG and load power. When K_r is set to 1.5, this parameter combination is above the islanding system stability boundary. As presented in Fig. 22, v_{dg} can still preserve stability at the grid-connected state, but it shows an oscillatory response in the islanding mode. After 1.83 seconds, the islanding condition is detected successfully. Furthermore, rising K_r to 13, this parameter combination is above the grid-connected stability boundary. As a result, after the IDM is enabled, Fig. 23 shows that the dc system loses stability even in grid-connected states. These three cases are evident that the practical boundaries are consistent with theoretical analysis.

C. Impact of DG and Load Power

Furthermore, the experimental and calculated dynamic responses of the PCC voltage with different system power are investigated in Fig. 24. It can be seen that the analytical

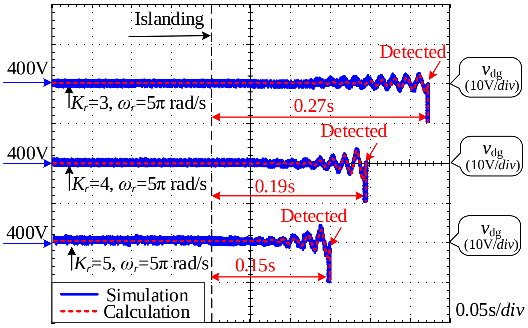

Fig. 25. Experimental and calculated dynamic responses with K_r increasing.

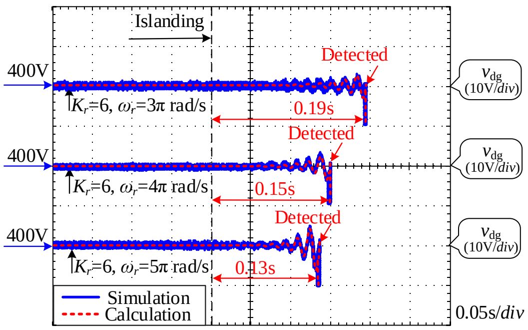

Fig. 26. Experimental and calculated dynamic responses with ω_r increasing.

waveform and experimental result are also well-fitted when both the DG and load power are low. It is also worth noting that the theoretical resonant frequency under 1.0 p.u, 0.75 p.u and 0. 5 p.u DG power are set as 65 Hz, 56 Hz, and 46 Hz, respectively. Under the power match condition, the oscillation frequency matches the theoretical value well. Moreover, as DG and load power decrease, the oscillation amplitude diverges faster, and thus the islanding detection time reduces. However, under power mismatch conditions, Fig. 24 shows that the PCC voltage is quickly shifted out of the undervoltage threshold without oscillation to indicate islanding, and the detection speed is significantly faster than that under power neutralization conditions. These cases further validate the correctness of time-domain simulation results under different power operating conditions.

D. Impact of Resonant Gain and Resonant Bandwidth

In this test, the impact of K_r and ω_r on islanding detection speed is investigated. The experimental waveforms and calculation results in the case of different K_r and ω_r are depicted in Fig. 25 and Fig. 26, respectively. As K_r varies from 3 to 5, it can be seen from Fig. 25 that the oscillation amplitude of v_{dg} becomes larger, and the islanding detection speed turns faster. In each case, the analytical trajectory fits well with the experimental waveforms. Similarly, with the rise of ω_r, the oscillation amplitude increases significantly, and thus the detection time is also decreased, as shown in Fig. 26. These results evident that both increasing K_r and ω_r are effective in improving the islanding detection speed.

E. Comparative Study

Furthermore, a comparative experiment is conducted to demonstrate the benefits of the proposed method in detection accuracy and detection time, as shown in Fig. 27. According

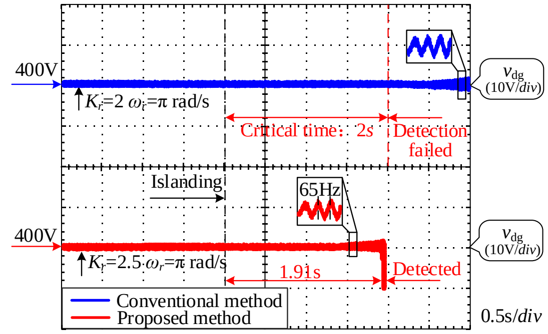

Fig. 27. Comparative experimental results of accuracy and detection time.

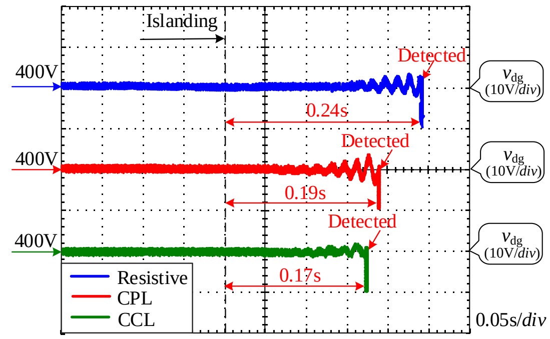

Fig. 28. Comparative experimental results under different load conditions.

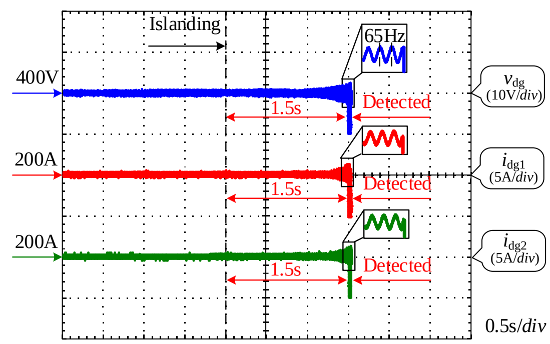

Fig. 29. Experimental results of a two-DG system.

to the Routh–Hurwitz criteria, K_r is set as 2, and ω_r is set as π rad/s, which can make the islanding system loses stability. However, the blue waveform in Fig. 27 shows that the islanding event cannot be detected in time because the detection speed is not accurately designed. Different from the conventional frequency domain method, after using the proposed method, it can be found that the critical value of K_r is 2.4 when ω_r is π rad/s to realize successful islanding detection within 2 seconds. Then, as K_r increases to 2.5, the red waveform in Fig. 27 indicates that the islanding can be detected within 2 seconds. In summary, the proposed method performs better in detection accuracy and detection time.

To validate the conservatism of the described parameter selection domain, three load conditions are tested in Fig. 28. It can be clearly seen that the detection time under both CPL and CCL conditions is much shorter than that under resistive load conditions as the pure resistance has the largest non-detection zone. These experimental results prove that the islanding detection parameter range obtained under resistive load conditions is also applicable to other load conditions.

F. Multiple Sources Test

In the end, a bus configuration of the dc microgrid with two DGs is investigated in the HIL platform to demonstrate the effectiveness of the described parameter selection domain. According to the previous analysis, when the ω_r of a single DG is designed as π rad/s, the critical value of K_r to achieve islanding detection within 2s is 2.4. On the other hand, with the same K_r and ω_r, the detection time of a two-DG system is much less than 2s, as shown in Fig. 29. This means that the islanding detection parameter boundary obtained in the basic single DG system is conservative and can also be applicable to a multi-source system.

VI. Conclusion

In this paper, a detection time calculation method is proposed based on the time-domain oscillation trajectory of PCC voltage to characterize the boundary of islanding detection parameters. Firstly, the steady-state dynamics of the PCC voltage in islanding modes are explored to reveal the limitations of the conventional frequency-domain-based islanding detection parameters design method. With the conventional method, there are always some values of resonant gain and resonant bandwidth which make the detection speed quite slow. The root cause of this problem is the stability boundary of the islanding system obtained in the frequency domain cannot consider the impact of detection time. On the basis of this, the characteristic equation of the islanding system is analyzed to simplify the expression of PCC voltage dynamics. Furthermore, the detection time calculation method is proposed based on the time-domain oscillation trajectory of PCC voltage. Under the detection time constraints, the boundary of the islanding detection parameters can be accurately depicted. In this manner, the effect of resonant parameters on the detection time can be evaluated quantitatively, while the fast detection speed is also guaranteed. In the end, the effectiveness and accuracy of the proposed method are verified by both time-domain simulations and hardware-in-loop experiments.

References

[1] A. Hirsch, Y. Parag, and J. Guerrero, "Microgrids: A review of technologies, key drivers, and outstanding issues," *Renew. Sustain. Energy Rev.*, vol. 90, pp. 402–411, Jul. 2018.

[2] H. Li, P. Ju, C. Gan, Y. Tang, Y. Yu, and Y. Liu, "Analytic estimation method of forced oscillation amplitude under stochastic continuous disturbances," *IEEE Trans. Smart Grid*, vol. 10, no. 4, pp. 4026–4036, Jul. 2019.

[3] R. B. Jafarabadi, J. Sadeh, J. D. J. Chavez, and M. Popov, "Two-level islanding detection method for grid-connected photovoltaic system-based microgrid with small non-detection zone," *IEEE Trans. Smart Grid*, vol. 12, no. 2, pp. 1063–1072, Mar. 2021.

[4] A. Dagar, P. Gupta, and V. Niranjan, "Microgrid protection: A comprehensive review," *Renew. Sustain. Energy Rev.*, vol. 149, pp. 1–20, Jul. 2021.

[5] M. Seyedi, S. A. Taher, B. Ganji, and J. Guerrero, "A hybrid islanding detection method based on the rates of changes in voltage and active power for the multi-inverter systems," *IEEE Trans. Smart Grid*, vol. 13, no. 6, pp. 2800–2811, Jul. 2021.

[6] M. Veysi, J. Aghaei, M. R. Soltanpour, M. Shasadeghi, B. Bahraniand, and D. J. Ryan, "Robust, accurate, and fast decentralized power sharing mechanism for isolated dc microgrid using droop-based sliding-mode control," *IEEE Trans. Smart Grid*, vol. 13, no. 6, pp. 4160–4173, Nov. 2022.

[7] V. A. Kleftakis, D. T. Lagos, C. N. Papadimitriou, and N. D. Hatziargyriou. "Seamless transition between interconnected and islanded operation of dc microgrids," *IEEE Trans. Smart Grid*, vol. 10, no. 1, pp. 248-256, Jan. 2019.

[8] J. Hu, Y. Shan, K. W. Cheng, and S. Islam, "Overview of power converter control in microgrids—challenges, advances, and future trends," *IEEE Trans. Power Electron*., vol. 37, no. 8, pp. 9907–9922, Aug. 2022.

[9] Y.C Jeung, D.C Lee, T. Dragičević, and F. Blaabjerg, "Design of passivity-based damping controller for suppressing power oscillations in DC microgrids," *IEEE Trans. Power Electron*., vol. 36, no. 4, pp. 4016–4028, Apr. 2021.

[10] M. Baranwal, A. Askarian, S. Salapaka, and M. Salapaka, "DC microgrids - part II: a review of power architectures, applications, and standardization issues," *IEEE Trans. Ind. Electron.*, vol. 66, no. 4, pp. 3082-3092, Apr 2019.

[11] M. A. Khan, A. Haque, V. S. B. Kurukuru, and M. Saad, "Islanding detection techniques for grid-connected photovoltaic systems-A review," *Renewable Sustain. Energy Rev.*, vol. 154, pp. 1–21, Feb. 2022.

[12] A. H. F. Jowzdani, I. Sadeghkhani, and A. M. Sani, "Islanding detection for dc microgrids based on episode of care severity index," *IEEE Trans. Smart Grid*, vol. 13, no. 2, pp. 954–961, Mar. 2022.

[13] N. A. Larik, M. F. Tahir, Z. M. S. Elbarbary, M. Z. Yousaf, and M. A. Khan, "A comprehensive literature review of conventional and modern islanding detection methods," *Energy Strategy Rev.*, vol. 44, pp. 1–17, Nov. 2022.

[14] *IEEE Standard for Interconnecting Distributed Resources With Electric Power Systems*, IEEE Std. 1547, 2003.

[15] H. R. Baghaee, D. Mlakić, S. Nikolovski, and T. Dragičević, "Antiislanding protection of PV-based microgrids consisting of PHEVs using SVMs," *IEEE Trans. Smart Grid*, vol. 11, no. 1, pp. 483–500, Jan. 2020.

[16] H. R. Baghaee, D. Mlakić, S. Nikolovski, and T. Dragičević, "Support vector machine-based islanding and grid fault detection in active distribution networks," *IEEE J. Emerg. Sel. Top. Power Electron*., vol. 8, no. 3, pp. 2385–2403, Sep. 2020.

[17] A. Makkieh, A. F. -James, D. Tzelepis, A. Emhemed, G. Burt, S. Strachan, and A. J. -Ferre, "Assessment of passive islanding detection methods for DC microgrids," in *Proc. 15th IET Int. Conf. AC DC Power Transmiss. (ACDC)*, 2019, pp. 1–6.

[18] C. N. Papadimitriou, V. A. Kleftakis, and N. D. Hatziargyriou, "A novel method for islanding detection in dc networks," *IEEE Transactions on Sustainable Energy*, vol. 8, no. 1, pp. 441–448, Jan 2017.

[19] B. K. Choudhury and P. Jena, "A digital lock-in amplifier assisted active islanding detection technique for dc microgrids," *IEEE Trans. Ind. Application.*, vol. 59, no. 1, pp. 377–391, Jan. 2023.

[20] B. K. Choudhury, and P. Jena, "Superimposed impedance-based passive islanding detection Scheme for DC microgrids," *IEEE J. Emerg. Sel. Topics Power Electron.*, vol. 10, no. 1, pp. 469–483, Feb. 2022.

[21] G. S. Seo, K. C. Lee, and B. H. Cho, "A new DC anti-islanding technique of electrolytic capacitor-less photovoltaic interface in DC microgrids," *IEEE Trans. Power Electron.*, vol. 28, no. 4, pp. 1632–1641, Apr. 2013.

[22] A. M. I. Mohamad and Y. A. R. I. Mohamed, "Assessment and performance comparison of positive feedback islanding detection methods in DC microgrids," *IEEE Trans. Power Electron.*, vol. 32, no. 8, pp. 6577–6594, Aug. 2017.

[23] Q. Huang, C. Li, H. Yang, Y. Dong, W. Li, X. He, W. Zhang, and J. Han, "Islanding detection methods based on self-oscillation of a particular frequency in DC distribution systems," in *Proc. IEEE Applied Power Electron Conf. Exposition. (APEC)*, 2020, pp. 574–580.

[24] Q. Huang, H. Chen, X. Xiang, C. Li, W. Li, and X. He, "Islanding detection with positive feedback of selected frequency for DC microgrid systems," *IEEE Trans. Power Electron.*, vol. 36, no. 10, pp. 11800–11817, Oct. 2021.

[25] T. Shi, H. Chen, B. Liu, S. Fan, F. Wang, X. Xiang, H. Yang, and W. Li, "Detection speed improvement and system stability enhancement for dc microgrids islanding detection based on impedance characteristic analysis," *IEEE Trans. Power Electron.*, vol. 38, no. 3, pp. 3785–3802, Mar. 2023.

[26] A. M. I. Mohamad and Y. A. I. Mohamed, "Impedance-based analysis and stabilization of active DC microgrids with positive feedback islanding detection schemes," *IEEE Trans. Power Electron.*, vol. 33, no.11, pp. 9902–9922, Mar. 2018.

[27] K. Jia, Z. Zhu, Q. Zhao, Z. Yang, and T. Bi, "Islanding detection method of multi-port photovoltaic DC micro grid based on harmonic impedance measurement," *IET Renew. Power Gener.*, vol. 13, no. 14, pp. 2604–2611, Oct. 2019.

[28] A. M. I. Mohamad and Y. A. I. Mohamed, "Analysis and mitigation of interaction dynamics in active DC microgrids with positive feedback islanding detection schemes," *IEEE Trans. Power Electron.*, vol. 33, no. 3, pp. 2751–2773, Mar. 2018.

[29] K. Ogata, *Modern Control Engineering*, 5th ed., Englewood Cliffs, NJ,USA: Prentice-Hall, 2010.

[30] T. Shi, X. Xiang, J. Lei, B. Liu, F. Wang, M. Chen, H. Yang, L. Li, and W. Li, "Non-detection zone elimination and detection speed improvement for dc microgrids islanding detection with adaptive resonant Frequency," *IEEE J. Emerg. Sel. Topics Power Electron.*, vol. 11, no. 6, pp. 5750–5765, Dec. 2023.

[31] S. Li, A. T. L. Lee, S. C. Tan, S. Y. R. Hui, "Plug-and-play voltage ripple mitigator for dc links in hybrid ac–dc microgrids with local bus-voltage control," *IEEE Trans. Ind. Electron.*, vol. 65, no. 1, pp. 687–698, Jan. 2018.

[32] H. Xiao, "A modular low current ripple electrolysis power supply based on multiphase half-bridge high-frequency inverters," *IEEE Trans. Power Electron.*, vol. 35, no. 10, pp. 10088–10096, Oct. 2020.

Tianling Shi (Student Member, IEEE) received the B.Sc. degree in electrical engineering and automation from the School of Electrical and Information Engineering, Jiangsu University, Zhenjiang, China, in 2018. He is currently pursuing the Ph.D. degree in electrical engineering with Shanghai University, Shanghai, China, and the University of Technology Sydney, Sydney, NSW, Australia, Collaborative Doctoral Research Degree Program.

From 2021 to 2023, he was a Visiting Researcher with the College of Electrical Engineering, Zhejiang University, Zhejiang, China. His research interests include the control and protection of dc microgrids.

Xin Xiang (Member, IEEE) received the B.Sc. degree from Harbin Institute of Technology, China in 2011, the M.Sc. degree from Zhejiang University, China in 2014 and the Ph.D. degree from Imperial College London, UK in 2018, all in Electrical and Electronic Engineering.

From 2018 to 2020, he was a Research Associate with Imperial College London. He is currently a tenure-track Associate Professor with the College of Electrical Engineering, Zhejiang University, Hangzhou, China. His research interests include the analysis and control of power electronics converters for power system applications.

Dr. Xiang was the recipient of the Eryl Cadwaladr Davies Prize for the Best Ph.D. Thesis of Electrical and Electronic Engineering Department, Imperial College London and the Best Ph.D. Thesis Award from IEEE PELS U.K. and Ireland Chapter.

Jintao Lei received the B.S. degree and Ph.D. degree in electrical engineering from the College of Electrical Engineering, Zhejiang University, Hangzhou, China, in 2018 and 2023, respectively. He is currently with the Corporate Research Center, Midea Group, Shanghai, China.

His research interests include the modeling and stability analysis of grid-connected power electronic converters.

Boxin Liu (Student Member, IEEE) received the B.Sc. degree in electrical engineering and automation in 2020 from the School of Electrical Engineering and Automation, Hefei University of Technology, Hefei, China. He is currently working toward the Ph.D. degree in electrical engineering at the College of Electrical Engineering, Zhejiang University, Zhejiang, China.

His research interests include the analysis and control of grid-connected power electronic converters.

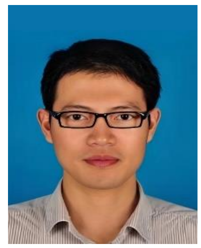

Fei Wang (Senior Member, IEEE) received the B.Sc. degree in electrical engineering and the M.Sc. degree in power electronics from Zhejiang University, Hangzhou, China, in 2002 and 2005, respectively, and the Ph.D. degree in power electronics from the Eindhoven University of Technology, Eindhoven, The Netherlands, in 2010.

He was with the Philips Lighting Electronics Global Development Center, Shanghai, China, from 2005 to 2006. He has been a Faculty Member with the School of Mechatronic Engineering and Automation, Shanghai University, Shanghai, since 2010, and became a Professor in March 2018. He has authored/co-authored more than 100 technical papers, one academic book, and also ten authorized invention patents. His current research interests include distributed generation, electrical drives, power quality, LED drivers, and smart grid.

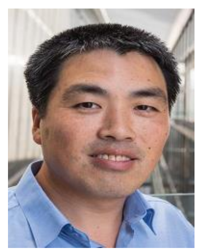

Li Li (Member, IEEE) received his B.S. degree from Huazhong University of Science and Technology in 1996, M.S. degree from Tsinghua University in 1999, and Ph.D. degree from University of California, Los Angeles in 2005 respectively, all in Electrical Engineering.

From 2005 to 2007 he was a research associate at the University of New South Wales at the Australian Defence Force Academy (UNSW@ADFA). From 2007 to 2011, he was a researcher at the National ICT Australia, Victoria Research Laboratory, Department of Electrical and Electronic Engineering, The University of Melbourne. He joined the University of Technology Sydney in 2011, and currently he is an Associate Professor. Dr Li held several visiting positions at various universities. His research interests are power systems and control theory. He is presently serving as an Associate Editor of IET Renewable Power Generation, IET Generation, Distribution and Transmission, and IET Smart Grid.

Ricardo P. Aguilera (Member, IEEE) received the B.Sc. degree in electrical engineering from the Universidad de Antofagasta, Antofagasta, Chile, the M.Sc. degree in electronics engineering from the Universidad Tecnica Federico Santa Maria, Valparaiso, Chile, and the Ph.D. degree in electrical engineering from the University of Newcastle (UoN), Newcastle, NSW, Australia, in 2003, 2007, and 2012, respectively.

From 2012 to 2013, he was a Research Academic with UoN, where he was part of the Centre for Complex Dynamic Systems and Control. From 2014 to 2016, he was a Senior Research Associate with the University of New South Wales, Sydney, NSW, Australia, where he was part of the Australian Energy Research Institute. Since September 2016, he has been with the School of Electrical and Data Engineering, the University of Technology Sydney, Ultimo, NSW, Australia, where he is currently a Senior Lecturer. His research interests include theoretical and practical aspects on model predictive control with application to power electronics, renewable energy integration, and microgrids.

Wuhua Li (Senior Member, IEEE) received the B.Sc. and Ph.D. degree in Power Electronics and Electrical Engineering from Zhejiang University, Hangzhou, China, in 2002 and 2008, respectively.

From 2004 to 2005, he was a Research Intern, and from 2007 to 2008, a Research Assistant in GE Global Research Center, Shanghai, China. From 2008 to 2010, he joined the College of Electrical Engineering, Zhejiang University as a Post doctor. In 2010, he was promoted as an Associate Professor. Since 2013, he has been a Full Professor at Zhejiang University. From 2010 to 2011, he was a Ryerson University Postdoctoral Fellow with the Department of Electrical and Computer Engineering, Ryerson University, Toronto, ON, Canada. He is currently the Executive Deputy Director of the National Specialty Laboratory for Power Electronics and the Vice Director of the Power Electronics Research Institute, Zhejiang University. His research interests include power devices, converter topologies and advanced controls for high power energy conversion systems. Dr. Li has published more than 300 peer-reviewed technical papers and holds over 50 issued/pending patents.

Due to his excellent teaching and research contributions, Dr. Li received the 2012 Delta Young Scholar from Delta Environmental & Educational Foundation, 2012 Outstanding Young Scholar from National Science Foundation of China (NSFC), 2013 Chief Youth Scientist of National 973 Program, 2014 Young Top-Notch Scholar of National Ten Thousand Talent Program, 2019 Distinguished Young Scholar from National Science Foundation of China. He serves as the Associated Editor of Journal of Emerging and Selected Topics in Power Electronics, IET Power Electronics, CSEE Journal of Power and Energy Systems, CPSS Transactions on Power Electronics and Applications, Proceedings of the Chinese Society for Electrical Engineering, Guest Editor of IET Renewable Power Generation for Special Issue “DC and HVDC system technologies”, Member of Editorial Board for Journal of Modern Power System and Clean Energy.

He received one National Natural Science Award and four Scientific and Technological Achievement Awards from Zhejiang Provincial Government and the State Educational Ministry of China. He was appointed as the Most Cited Chinese Researchers by Elsevier since 2014.